Control Engineering

Ashish Tewari

Aeroservoelasticity

Modeling and Control

Birkhäuser

Control Engineering

For further volumes:
http://www.springer.com/series/4988

Ashish Tewari

Aeroservoelasticity

Modeling and Control

Birkhäuser

Ashish Tewari
Department of Aerospace Engineering
Indian Institute of Technology, Kanpur
Kanpur
Uttar Pradesh
India

ISSN 2373-7719 ISSN 2373-7727 (electronic)
Control Engineering
ISBN 978-1-4939-2367-0 ISBN 978-1-4939-2368-7 (eBook)
DOI 10.1007/978-1-4939-2368-7

Mathematics Subject Classification (2010): 70Q05, 74H10, 74H15, 74F10, 74S05, 74S25, 76G25, 76H05, 76J20, 76M22, 76M23, 76M25, 76M40, 93B15, 93B30, 93B36, 93B52, 93B55, 93C05, 93C10, 93C15, 93C35, 93C40, 93C80, 93D05, 93D20, 32D99

Library of Congress Control Number: 2015933384

Springer New York Heidelberg Dordrecht London

Printed on acid-free paper

Springer is part of Springer Science+Business Media (www.springer.com)

To the order and beauty of nature,
and its finely crafted control laws.

Preface

This book presents aeroservoelasticity (ASE) as a well-formed discipline with a systematic framework. While many research articles have appeared on the special applications of ASE–such as active flutter suppression and gust load alleviation–there are no textbooks and monographs on the general and systematic procedure to be followed in the modeling and analysis of aeroservoelastic systems. This book is a first step in trying to fill this important gap in the aerospace engineering literature. This book introduces the basic math modeling concepts and highlights important developments involved in structural dynamics, unsteady aerodynamics, and control systems. It also attempts to evolve a generic procedure to be applied for ASE system synthesis. The treatment includes finite-element structural modeling and detailed unsteady aerodynamic modeling at various speeds for deriving the necessary aeroelastic plants, with sample control applications to active flutter suppression, load alleviation, and adverse ASE coupling.

A general aeroelastic plant is derived via the finite-element structural dynamic model, unsteady aerodynamic models for various regimes in the frequency domain, and the associated state-space model by rational function approximations. For more advanced models, the full-potential, Euler, and Navier – Stokes methods for treating transonic and separated flows are also briefly addressed. Essential ASE controller design and analysis techniques are introduced to the reader. Introduction to robust control-law design methods of LQG/LTR and H_2/H_∞ synthesis is followed by a brief coverage of nonlinear control techniques of describing functions and Lyapunov functions.

The fundamental concepts are presented in such a way that the most important features can be easily deduced. The breadth of coverage is sufficient for a thorough understanding of ASE.

The focus of this book is on aeroservoelastic modeling, including a brief presentation on robust and optimal control methods that can be applied to important aeroservoelastic design problems. It is not possible to give a more comprehensive ASE treatment in a single book, and it is envisaged that a future book can be devoted to more advanced topics such as adaptive and nonlinear control design techniques.

This book is aimed at graduate students and advanced researchers in aerospace engineering, as well as professional engineers, technicians, and test pilots in the aircraft

industry and laboratories. The reader is assumed to have taken basic undergraduate courses in mathematics and physics—particularly calculus, complex variables, linear algebra, and fundamental dynamics—and is encouraged to review these concepts at several places in the text.

A book on ASE is difficult to write due to the breadth of topics it must necessarily address. While this book covers the essentials of modeling aspects of ASE with some control applications, it gives sufficient motivation to a reader with specific research interests to further explore the relevant topics. Furthermore, the treatment of topics is such that a novice can quickly build up his/her understanding of ASE without much difficulty. References are selected keeping both the types of readers in mind.

This book has been long in writing, with the intention first having occurred to the author about 15 years ago. Not having access to the industrial codes for finite-element and unsteady aerodynamics necessary for building such an exposition, and not finding the time to write one's own codes, the project continued to be delayed until about 2 years ago, when courage was finally gathered for this purpose. Testing and validating the codes for the many examples in the book was itself a formidable task, which required many hours of patient programming.

I would like to thank Walt Eversman for his course on aeroelasticity, and for advising me in my graduate studies. The editorial and production staff of Birkhäuser have offered many constructive inputs during the preparation of the manuscript, for which I am indebted to them. I am also grateful to The MathWorks, Inc. for providing the latest MATLAB/Simulink version utilized for the examples throughout the book.

November 2014 Ashish Tewari

Contents

Chapter 1
Aeroservoelasticity

1.1 Introduction

Aeroservoelasticity (ASE) is the interface of unsteady aerodynamics, structural dynamics, and control systems, and is an important interdisciplinary topic in aerospace engineering. It is a study of dynamic interactions among air loads, structural deformations, and automatic flight control systems commonly experienced by the modern aircraft. The relevance of ASE to modern airplane design has increased considerably with the advent of flexible, lightweight structures, increased airspeeds, and closed-loop automatic flight control. Since aeroservoelasticity lies at the interface of aerodynamics, structures, and control, its impact on aircraft design and operation requires a thorough understanding of these core areas as far as they contribute to building an accurate mathematical model (Fig. 1.1).

While aeroelastic interactions have been studied for nearly a century, the impact of an active control system on dynamic aeroelasticity is a relatively new topic, and has come into focus with the advent of modern fly-by-wire designs. In such aircraft, the controller bandwidth can encroach the upon aeroelastic modal spectrum, thereby leading to resonance-like behavior in certain flight conditions. The most common example of such an interaction between the control and aeroelastic systems is the closed-loop flutter—a catastrophic dynamic coupling between the elastic motion, the unsteady aerodynamic loading, and a controller-actuated surface. Many airplane accidents (such as Taiwan IDF fighter and Lockheed YF-22 prototypes) have been blamed on unforeseen and unstable ASE couplings. In order to understand how such a phenomenon can remain unforeseen in the modern technical era, let us consider a well-designed car with the best engine, chassis, and electronics, and thoroughly tested for the most adverse road conditions that can be expected. However, when put into production, the same car could experience poor performance and even engine stalling due to a minor feature such as cable routing. In such a case, engine vibration at a certain speed can interact with the natural frequency of one of the spark plug cables, thereby leading to its coming loose and causing an even greater engine vibration. The engine controller would detect the poor combustion as a lean or cold mixture condition, and try to correct it by increasing the fuel volume injection. The

A. Tewari, *Aeroservoelasticity,* Control Engineering,
DOI 10.1007/978-1-4939-2368-7_1

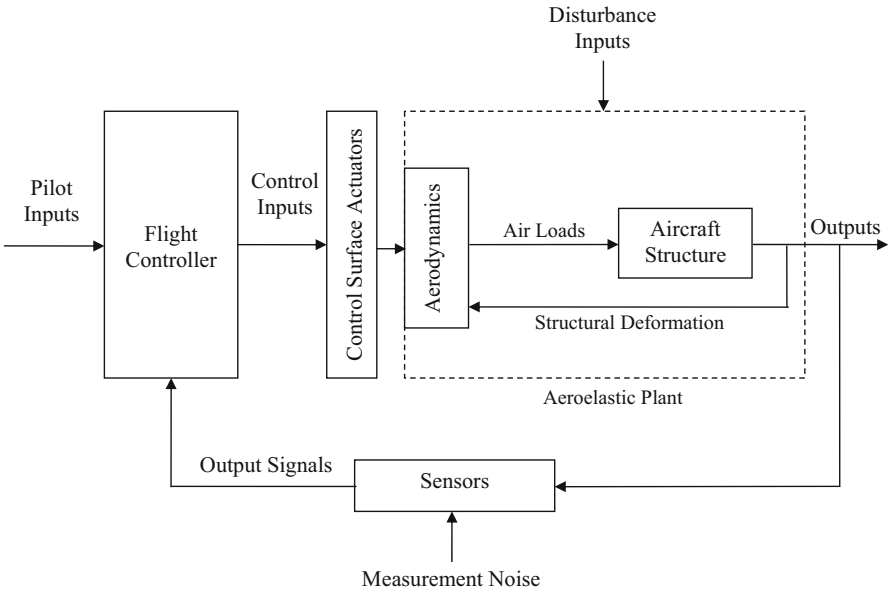

Fig. 1.1 Block diagram of a typical aeroservoelastic system

result would be an even rougher idle with black smoke, fouled spark plugs and injectors, and possibly an engine failure. Troubleshooting such a condition would be a nightmare, and the fix is either an expensive redesign of the engine, a reprogramming of the fuel controller, or an identification and change of the culprit natural frequency by merely redesigning the cable routings and clamps. If a mathematical model is constructed of such a dynamic interaction between electromechanical connectors, fuel control system, and engine dynamics, such a model is likely to be a formidable interdisciplinary exercise.

ASE is a fledgling discipline when compared to the other traditional aerospace areas of aerodynamics, structures, propulsion, and flight mechanics. Its formal beginning can be traced to the early 1970s, when ways of addressing the problem of flutter were being investigated in earnest due to the several new aircraft designs evolving in that era. Highly maneuverable fighters such as the Lockheed F-16 and the McDonnell Douglas F/A-18, as well as efficient passenger transports such as the Boeing-767 and the Airbus A-320 that were being developed, had inbuilt automatic flight control systems, which could be programmed relatively easily to achieve secondary tasks, such as active flutter suppression and maneuver/gust load alleviation. Prior to that era, a passive redesign of the structural components was the only way to avoid flutter, whose analysis often required thousands of hours of painstaking and dangerous flight flutter testing, and wind-tunnel tests of aeroelastically scaled models, thereby increasing the already high costs of prototype development. Consequently, flutter analysis and prevention was a stumbling block in developing novel aircraft configurations.

In order to overcome the inadequacy of passive techniques, and to fly at a velocity greater than the open-loop flutter velocity for greater speed and efficiency, the concept of active flutter suppression was developed in the 1970s [2, 3, 126, 143, 152]. Herein, an automatic control system actuates a control surface on the wing, in response to the structural motion sensed by an accelerometer, which increases the flutter speed in a closed loop by changing the stability characteristics of the open-loop system.

Active flutter suppression requires accurate knowledge of the aeroelastic modes that cause flutter, which are then actively changed in such a way that closed-loop flutter occurs at a higher flight velocity. Although the classical flutter of a high aspect-ratio wing—such as that of a Boeing 747 or an Airbus A-380—is caused by an interaction between the primary bending and torsion aeroelastic modes, the flutter mechanism of a low aspect-ratio wing, such as that of an F/A-18 (or F-22) fighter airplane is rather more complicated, comprising a coupling of several higher aeroelastic modes. In order to actively suppress flutter, it is necessary that an accurate aeroelastic model based on modeling of the unsteady aerodynamic forces as a transfer matrix be derived. The most common method of obtaining the unsteady aerodynamic transfer matrix is the use of optimized rational function approximations [43, 50, 85, 175] for its terms, fitted to the frequency-domain aerodynamic data in the harmonic limit. After the transfer matrix is derived, a linear, time-invariant, state-space model for the aeroelastic system, including the control surface actuators, can be obtained. The multivariable feedback controller for active flutter suppression can then be designed by standard closed-loop techniques, such as eigenstructure assignment and linear optimal control [168]. Since it is crucial that the derived control laws must be robust with respect to modeling uncertainties and measurement noise in a wide range of operating conditions, robust and adaptive controllers are specially sought for a practical application.

The first practical demonstration of active flutter suppression was carried out by the US Air Force in 1973 in their Load Alleviation and Mode Stabilization (LAMS) program, which resulted in a Boeing B-52 bomber flying 10 knots faster than its open-loop flutter velocity. This was accompanied by flight flutter testing of aeroelastic drones under NASA-Langley's Drones for Aeroelastic Testing (DAST) program. These pioneering developments in active flutter suppression received an impetus at NASA-Langley and Ames laboratories [4, 5, 118, 122] with novel control laws developed at Ames being tested and further developed in Langley's transonic dynamics wind tunnel. These developments in the 1970s were greatly enabled by the optimal control theory advancements [131, 163] of that era. ASE design and analysis efforts continued in the 1980s and 1990s [116, 117, 191], which were given a further boost by the newly developed robust multivariable control theory [62, 108]. Buoyed by their early achievements in active flutter suppression, the US Air Force and Rockwell, initiated the ambitious Active Flexible Wing (AFW) program [113, 127], wherein the objective was to utilize favorable aeroservoelastic interactions to produce performance, stability, and control improvements on a highly flexible and overly instrumented wind-tunnel wing model, employing multiple control surfaces and gain scheduled control laws. The survey paper of Mukhopadhyay [119] gives an excellent overview of how the seemingly independent technical developments over

the preceding half century in the otherwise disparate areas of structural dynamics, unsteady aerodynamics, and control systems, converged and came into a sharp focus in the field of aeroservoelasticity. An offshoot of aeroservoelastic design is the evolving area of multidisciplinary optimization for synthesizing lightweight wing structures [102], an example of which was the first forward-swept wing experimental prototype, the Grumman X-29A [65].

The main challenge in ASE mathematical analysis and design is in deriving a suitable unsteady aerodynamic model of aircraft wings and tails (or canards). The aeroelastic plant for flutter suppression of a thin wing-like surface is derived at subsonic and supersonic speeds using small-disturbance, potential aerodynamic models [7, 21, 61, 194, 180, 181] with a harmonic (frequency response) theory. Such a model is linear, and can be directly employed in developing an aerodynamic transfer matrix, and finally a linear, time-invariant state-space model through analytic continuation in the Laplace domain. However, there are important flow regimes where such a linearized model is inapplicable. The ASE applications which involve unsteady separated flows and transonic shock-induced flows, are inherently nonlinear in nature and require advanced computational fluid dynamics (CFD) modeling techniques [45, 166]. An example of nonlinear aeroelasticity is the post-stall buffet arising due to a sudden and large increase in the angle of attack, either by an abrupt maneuver, or a vertical gust. The ASE plant for such a case is further complicated by the separated wake and/or leading-edge vortex from the wing interacting with the tail, resulting in an irregular and sometimes catastrophic deformation of the tail—either on its own or driven by rapid and large deflections of the elevator. Such a wing-tail-elevator coupling of a post-stall buffet, or a shock-vortex interaction requires a fully viscous flow modeling that is only possible by a Navier–Stokes method. Another example of nonlinear ASE is the control of unsteady control surface buzz and shock-induced flow separation encountered by an aircraft maneuvering in the transonic regime, leading to nonlinear flutter or limit-cycle oscillation (LCO) [18, 99]. An appropriate CFD model in such a case would require a full-potential code [73, 162], coupled inviscid/boundary-layer method [46], or a Navier–Stokes method [123, 195], depending upon the geometry, structural stiffness, Mach number, and Reynolds number. Sometimes, semiempirical models are devised from wind-tunnel test results for separated and shock-induced flows [47, 156], because they do not require unsteady CFD computations to be performed in loop with structural dynamic and control-law calculations. However, the veracity of such a correlation must be checked carefully before being deployed in ASE design and analysis. The use of CFD models (Euler/Navier–Stokes) to derive linearized aerodynamic transfer functions/matrices has also been suggested in the literature [12, 136, 197]. This is evidently aimed at using the same linearized model for a range of flight conditions (Mach number, angle of attack, etc.) rather than having to repeat a CFD computation for every such condition. The coefficients of the approximation can be adjusted by an auto-regressive moving average (ARMA) model [137, 197], which brings such a method quite close to an adaptive control application (albeit in the open loop). However, approximating a nonlinear system by a linear transfer function can be inaccurate, even in a narrow range of operating conditions. An alternative method is

to employ flight-test data for deriving an ASE model, such as the neural-network identification method proposed by Boely and Botez [26].

Transonic flutter/buffet analysis is fraught with shock-induced oscillations, and is thus inherently nonlinear. It is also crucial in the aeroelastic stability analysis of most of the modern transport type aircraft, because their cruising speeds are just under the sonic speed. Fortunately, the nonlinear effects of transonic flutter are accurately captured by a transonic small-disturbance (TSD) model, even for a thick supercritical wing [176, 199] of a modern airliner. This fact offers the promise of coupling the aeroelastic stability analysis with a TSD code [14, 37, 76]. Alternative methods proposed for the time-linearized (low-frequency) transonic case involve a field-panel TSD method [105], or a full-potential method [130] applied in a doublet-lattice [61] type calculation of aerodynamic influence coefficients relating the pressure and normal velocity (upwash) in the harmonic limit. However, while such an approach can be applied to relatively lower natural frequencies of the primary bending and torsion modes of a high aspect-ratio wing (like that of a modern subsonic airliner), the concept of time linearization would fail when applied to the much higher frequencies of a low aspect-ratio, fighter-type wing, which is much stiffer in both bending and torsion.

Despite the early successes in demonstrating active flutter suppression/load alleviation, ASE has remained largely an experimental area [151] and has still not reached operational status on any aircraft. This remarkable failure is mainly due to the difficulty of designing a multivariable control system, which is sufficiently robust to the parametric uncertainties in the underlying unsteady aerodynamic model. Clearly, the aircraft designers and operators are reluctant to take risks until (what might be considered) suitably reliable ASE modeling and analysis methods become prevalent.

Due to the inherent uncertainty of an unsteady aerodynamic model, a closed-loop controller for ASE application must be quite robust to modeling errors. Furthermore, such a controller must also adapt to changing flight conditions. Hence, an ASE control law must not only be robust, but also self-adaptive, which renders it mathematically nonlinear even for a linear aeroelastic plant of the subsonic and supersonic regimes. Furthermore, designing a control law based upon nonlinear aeroelastic iterative models can be a very cumbersome and computationally intensive process. Instead, adaptive control techniques can be used for extending the subsonic and supersonic linear feedback designs to predict and suppress the transonic flutter. Adaptive control has been an area of active research in the past few decades [10, 89], and many useful design techniques have emerged that can be applied to ASE. However, these remain "application specific" (rather than general), if not completely ad hoc in many cases. Thus, ASE control-law derivation for a particular case is as challenging as the problem of aeroelastic modeling. For this reason, ASE has remained a formidable technological problem. For a linear aeroelastic plant, a high-gain linear feedback generally gives robustness with respect to modeling uncertainties in the control bandwidth, but degrades the response to the high-frequency measurement noise. Several linear feedback strategies are in vogue for striking a compromise between robustness to plant uncertainty and noise rejection. These include the linear

quadratic Gaussian (LQG) compensation with loop-transfer recovery (LTR) [108], H_2/H_∞ control [64], and structured singular value synthesis [30, 42].

Separated and shock-dominated flows nonlinearly interact with the aircraft structure, resulting in unstable oscillations, hysteresis, or limit cycles. While there are some papers and monographs on nonlinear aeroelastic modeling, such as Dowell and I'lgamov [41], their emphasis is on structural nonlinearities rather than on aerodynamic ones. Furthermore, the control aspects of ASE are seldom covered in such articles. Thus it is important to include nonlinear aerodynamic effects in a discussion on ASE, which is one of the tasks of this book. Control of nonlinear aeroelastic plants requires either describing function approximations [158, 182], Lyapunov-based controllers [60, 132], feedback linearization [78], or a sliding-mode (variable structure) control [53]. Furthermore, the issue of robustness is important for nonlinear plants [77]. Adaptation of controller parameters for both linear and nonlinear plants introduces a further complexity in the ASE design and analysis, and can be handled by gain scheduling, self-tuning regulation, model reference adaptive laws [10], or recursive backstepping [89], depending upon the specific application. There is little mathematical treatment of nonlinear ASE effects in the literature, and a future book is planned to cover this important gap.

The present book is a monograph on the basic concepts relevant to ASE modeling and analysis. Chapter 2 addresses the problem of basic structural modeling, whereas Chap. 3 is largely devoted to the techniques employed in deriving frequency-domain (or harmonic) aerodynamics of low-speed, subsonic, transonic, and supersonic flight regimes. It also covers the discussion of unsteady vortex-lattice model as an example of a simple potential flow model that can be applied to large amplitude movements (flapping) of an airfoil with thickness and camber. Such a treatment is somewhat a departure from what is considered the traditional aerodynamics of an oscillating flat-plate wing, which is commonly used in most linearized ASE models. The objective of such a model is its possible application in flapping-wing flight. Chapter 4 is concerned with the derivation of transient aerodynamic models by rational function approximations (RFA) that can be readily converted to state-space, linear time invariant (LTI) aeroelastic models. Chapter 5 is a presentation of linear control law derivation and analysis techniques, with some typical aeroseroelastic application examples. Finally, Chap. 6 is a discussion of nonlinear ASE topics. The chapters are organized in such a way that a reader can directly go to a specific topic without having read a previous one. However, for comprehensive understanding, it would be ideal to read the chapters sequentially. A basic knowledge of aerodynamics and control theory is assumed of the reader. Furthermore, familiarity with numerical methods [111, 154, 165] will also be helpful. The reader will find the bibliography arranged alphabatically, and thus easy to refer to. While it is impossible to list all the relevant references on this active and productive research topic, some thought has been applied to select useful articles for the benefit of the reader.

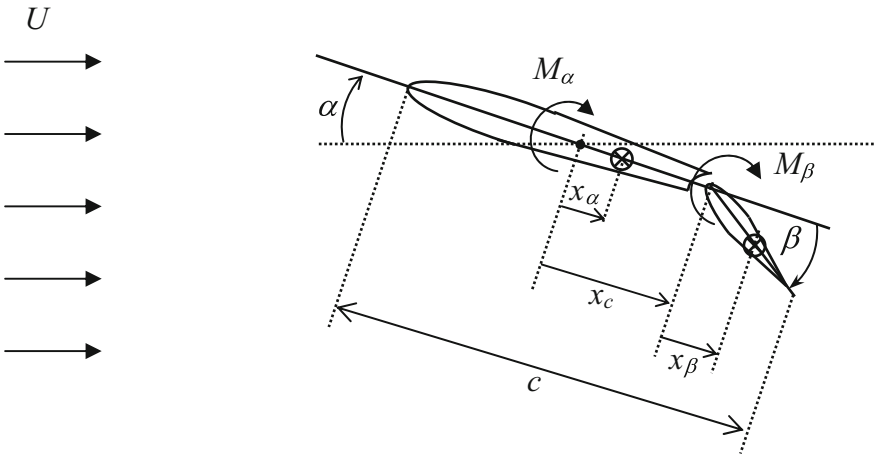

Fig. 1.2 A pitching airfoil with trailing-edge control surface

1.2 An Illustrative Example

While the general aeroelastic motion of an aircraft wing involves many degrees of freedom (Chap. 2), in order to illustrate the concept of aeroservoelasticity, let us consider a two-dimensional wing section (airfoil) that can only rotate about a fixed axis by an angle α (called the angle of attack). The airfoil is equipped with a trailing-edge control surface that can rotate by an angle β relative to the airfoil's chord plane, as shown in Fig. 1.2. The entire setup is mounted on a frictionless torsional spring of stiffness k_α, whereas the control surface hinge is also frictionless and has a rotational spring of stiffness k_β. The hinge line of the control surface is located at a distance of x_c behind the pitch axis. The mass of the control surface is m_c, and the distance of the control surface's center of mass behind its own hinge line is x_β (Fig. 1.2). The moment of inertia of the setup about the pitch axis is I_α, whereas that of the control surface about its hinge is I_β. The setup is placed in a uniform, incompressible flow of speed U and density ρ. The control surface is equipped with a direct current (DC) motor that can apply a torque u about the control surface hinge line relative to the airfoil. The linearized equations of motion of the structure can be expressed as follows, by either Newton's second law, or the energy approach:

$$\mathsf{M}\ddot{\mathbf{q}} + \mathsf{K}\mathbf{q} = \mathbf{Q} + (0,\ 1)^T u, \tag{1.1}$$

where $\mathbf{q} = (\alpha, \beta)^T$ is the generalized coordinates vector, $\mathbf{Q} = (M_\alpha, M_\beta)^T$ is the generalized air loads vector, and M, K are the following generalized mass and stiffness matrices, respectively, of the structure:

$$\mathsf{M} = \begin{pmatrix} I_\alpha & m_c x_c x_\beta \\ m_c x_c x_\beta & I_\beta \end{pmatrix}, \tag{1.2}$$

$$\mathsf{K} = \begin{pmatrix} k_\alpha & 0 \\ 0 & k_\beta \end{pmatrix}. \tag{1.3}$$

The generalized aerodynamic loads vector consists of the pitching moment M_α, and the control surface hinge moment M_β. For simplicity, it is assumed that the aerodynamic moments can be modeled primarily as first-order lag (or circulatory) effects of the unsteady wake shed by the airfoil, as well as the noncirculatory contributions of the aerodynamics to inertia (called the *apparent mass* effect), damping, and stiffness. Such a model of unsteady aerodynamics is given by the following relationship in the Laplace domain:

$$\mathbf{Q}(s) = \frac{1}{2}\rho U \left(a_1 + a_2 s + \frac{a_3 s}{s+b} \right) \begin{Bmatrix} A_1 \\ A_2 \end{Bmatrix} w(s), \tag{1.4}$$

where s represents the Laplace variable, and $w(s)$ is the following upwash (flow velocity component normal to the wing) at a specific location on the airfoil:

$$w(s) = (C_1,\ C_2,\ C_3,\ C_4) \begin{Bmatrix} \mathbf{q}(s) \\ s\mathbf{q}(s) \end{Bmatrix}, \tag{1.5}$$

and $A_1, A_2, a_1, \ldots, a_3, b, C_1, \ldots, C_4$ are constant aerodynamic parameters (in addition to ρ and U). Equations (1.4) and (1.5) result in the following relationship for the generalized unsteady aerodynamic loads:

$$\mathbf{Q}(s) = \mathsf{G}(s) \begin{Bmatrix} \mathbf{q}(s) \\ s\mathbf{q}(s) \end{Bmatrix}, \tag{1.6}$$

where the aerodynamic transfer matrix is given by

$$\mathsf{G}(s) = \frac{1}{2}\rho U \left(a_1 + a_2 s + \frac{a_3 s}{s+b} \right) \begin{Bmatrix} A_1 \\ A_2 \end{Bmatrix} (C_1,\ C_2,\ C_3,\ C_4)\,. \tag{1.7}$$

The simple aeroelastic model considered here leads to a state-space representation given as follows:

$$\dot{\mathbf{x}} = \mathsf{A}\mathbf{x} + \mathsf{B}u, \tag{1.8}$$

$$y = \alpha = \mathsf{C}\mathbf{x} + \mathsf{D}u, \tag{1.9}$$

where $\mathbf{x} = (\mathbf{q}^T, \dot{\mathbf{q}}^T, x_a)^T$ is the state vector,

$$\mathsf{A} = \begin{bmatrix} 0 & \mathsf{I} & 0 \\ -\bar{\mathsf{M}}^{-1}\bar{\mathsf{K}} & \bar{\mathsf{M}}^{-1}\bar{\mathsf{C}}_d & -\frac{1}{2}\rho U b a_3 \bar{\mathsf{M}}^{-1} \begin{Bmatrix} A_1 \\ A_2 \end{Bmatrix} \\ (C_1,\ C_2) & (C_3,\ C_4) & -b \end{bmatrix}, \tag{1.10}$$

$$\mathsf{B} = \begin{bmatrix} 0 \\ \bar{\mathsf{M}}^{-1}(0,\ 1)^T \\ 0 \end{bmatrix}, \tag{1.11}$$

$$\mathsf{C} = (1,\ 0,\ 0,\ 0\ 0)\,; \qquad \mathsf{D} = 0, \tag{1.12}$$

$$\bar{\mathsf{M}} = \mathsf{M} - \frac{1}{2}\rho U a_2 \begin{Bmatrix} A_1 \\ A_2 \end{Bmatrix} (C_3,\ C_4)\,, \tag{1.13}$$

$$\bar{\mathsf{C}}_d = \frac{1}{2}\rho U \begin{Bmatrix} A_1 \\ A_2 \end{Bmatrix} [a_2(C_1,\ C_2) + (a_1 + a_3)(C_3,\ C_4)]\,, \tag{1.14}$$

$$\bar{\mathsf{K}} = \mathsf{K} - \frac{1}{2}\rho U(a_1 + a_3) \begin{Bmatrix} A_1 \\ A_2 \end{Bmatrix} (C_1,\ C_2)\,. \tag{1.15}$$

The matrices $\bar{\mathsf{K}}, \bar{\mathsf{C}}_d, \bar{\mathsf{M}}$ are the generalized stiffness, damping, and mass matrices of the aeroelastic system, which reduce to $\mathsf{K}, \mathsf{0}, \mathsf{M}$, respectively, for the in vacuo case ($\rho = 0$). It is to be noted that the order of the aeroelastic system is increased by one due to the aerodynamic state, $x_a(t)$, arising out of the lag term, $a_3 s/(s + b)$, which augments the (last row and column of the) dynamics matrix A. The given aeroelastic plant is controllable with the motor torque input, which can be verified from the rank of the controllability test matrix for the pair (A, B) [168].

The aeroelastic stability is determined from the eigenvalues of A:

$$| s\mathsf{I} - \mathsf{A} | = 0$$

at a certain flight condition. Let $I_\alpha = 10, I_\beta = 1\ \text{kg m}^2$, $k_\alpha = 40, k_\beta = 9\ \text{N m/rad}$, $m_c = 0.1$ kg, $x_c = 0.3\,\text{m}$, $x_\beta = 0.1\,\text{m}$, and the aerodynamic parameters be the following:

$$\rho = 1.225\ \text{kg/m}^3\ ;\ \ A_1 = 0.5\ ;\ \ A_2 = -0.0268,$$

$$C_1 = 1.0\ ;\ \ C_2 = 0.7067\ ;\ \ C_3 = 0.5\ ;\ \ C_4 = 0.3387,$$

$$a_1 = 1.0\ ;\ \ a_2 = 0\ ;\ \ a_3 = -2.0\ ;\ \ b = 0.05.$$

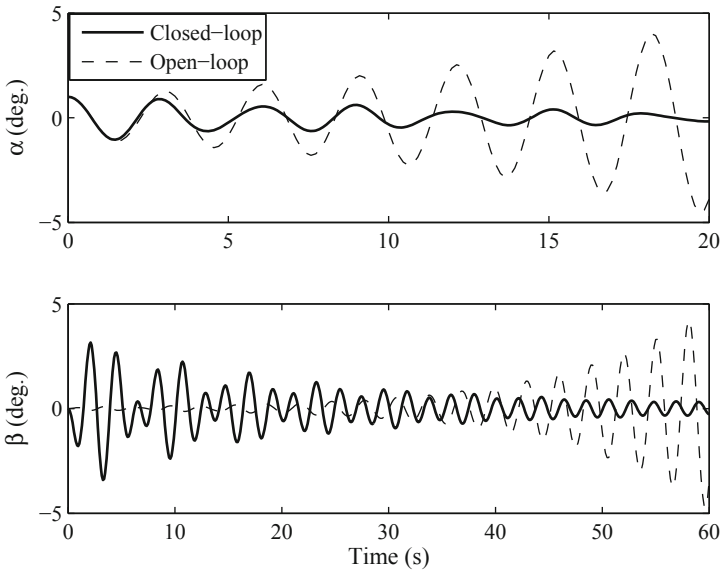

Fig. 1.3 Initial reponse of a pitching airfoil with trailing-edge control surface and a linear feedback control law

It can be easily shown that the aeroelastic plant is unstable at any speed U due to the unsteady aerodynamic characteristics associated with the wake (modeled here as a simple time lag).

In order to stabilize the plant, the following linear feedback control law is tried for $U = 10\,\mathrm{m/s}$:

$$u = -(8.2703,\ 0.4301,\ -3.2839,\ 0.3131) \begin{Bmatrix} \alpha \\ \beta \\ \dot{\alpha} \\ \dot{\beta} \end{Bmatrix}.$$

This feedback control law stabilizes the closed-loop system, which is shown by the initial response to a unit angle-of-attack perturbation (caused by a vertical gust) plotted in Fig. 1.3. For a practical implementation of such a control law, there must be angle and rate sensors mounted on the airfoil pitch axis and the control surface hinge line, whose combined electrical signals are fed to a multichannel amplifier for driving the control surface motor. Alternatively, a single output y can be selected, which results in a linear combination of all the state variables. Such an output could be the normal acceleration measured by an accelerometer placed at a point on the control surface (the reader can show such a plant will be observable [168]). However, the derivation of the control law in that case will require the design of an observer, which can reconstruct the information about the state variables from the knowledge

of the input u and the output y. The reader is advised at this point to refresh the definitions of stability, controllability, and observability of linear systems [84].

The gains of the amplifier—indicated above for $U = 10\,\mathrm{m/s}$—can be individually adjusted with a changing flight speed U (or atmospheric density ρ), until the desired closed-loop response is obtained. An adjustment of the controller gains with a changing operating condition is called adaptation. Instead of a human operator, a separate control system—called adaptation mechanism—can be devised such that the gains are automatically adjusted to the correct values with changing flight speed and density. Such a control system which has the capability of self-modification in order to always achieve the desired closed-loop behavior is called an adaptive control system. A modern flight control system has an inbuilt adaptive mechanism, which can sense a change in the flight condition by pressure and temperature sensors, and applies a correction to the feedback gains.

Chapter 2
Structural Modeling

2.1 Introduction

Aircraft have thin-walled, built-up structures for high strength-to-weight ratio and stiffness. The transverse and longitudinal members share the external loads with the outer skin panels in a semimonocoque construction. It would appear that an analysis of such a structure requires a detailed model of each component, which specifies the exact manner in which it is connected to the other members. Such a modeling would be a daunting task, requiring enormous computational resources. Fortunately, although a detailed analysis of individual structural components is indeed necessary for structural design, it is not required for aeroelastic purposes where some simplifying approximations can be made. Many aircraft components—such as the wings and the fuselage—are designed to be slender and streamlined for a high lift-to-drag ratio. The associated structures thus have small thicknesses and can be often idealized as either solid beams or plates. Furthermore, the necessity of preserving aerodynamic shape results in a much higher bending stiffness in the transverse (chordwise or radial) direction, compared with that in the longitudinal (lengthwise or spanwise) direction, which is achieved in practice by closely spaced ribs and frames. The resulting assumption of chordwise rigidity is quite valuable in reducing the degrees of freedom for a structural model. However, such a model would be inaccurate for wings with very small aspect ratio where chordwise and spanwise bending stiffnesses would be comparable. Another major simplification is the fact that any inelastic deformation leading to buckling of skin panels under design loads is unacceptable from aerodynamic design viewpoint. Therefore, an elastic stress–strain behavior is necessary, and results in a linear load–displacement relationship—a valuable model from aeroelastic perspective. However, post-buckling behavior of skin panels requires nonlinear structural modeling, which is excluded from usual aeroelastic design and analysis.

The main emphasis of an aeroelastic model is upon wing-like structures, which are quite thin in comparison with the chord and span. This offers a valuable modeling simplicity, which combined with the chordwise rigidity of high aspect-ratio wings, results in plane cross-sections remaining essentially plane due to a free warping of the structure under twisting loads. Conversely, a bending load would not produce any twisting deformation due to the same reason. Hence by Saint-Venant's theory [68],

A. Tewari, *Aeroservoelasticity,* Control Engineering,
DOI 10.1007/978-1-4939-2368-7_2

one can decouple bending and torsion, thereby leading to the very useful concepts of shear center and elastic axis. Of course, such a decoupling is not possible for either short beams, or plate-like structures where sectional warping invariably causes some normal (bending) stresses. Furthermore, if shear deformations can be neglected due to an essentially thin beam, the bending deformations can be treated by a simple Euler–Bernoulli beam theory.

2.2 Static Load Deflection Model

Consider an elastic wing with an unloaded and undeformed mean surface defined by $z = s(x, y)$ and generated by smoothly joining the wing's chord lines, camber lines, or any other centroidal features of the cross-sections. If a concentrated load, $\mathbf{P}$, is now applied at a point, (ξ, η), located on the original mean surface, it will cause a structural deflection, $\boldsymbol{\delta}(x, y)$ such that a new equilibrium is achieved in the deformed configuration given by the deformed surface, $z = s'(x, y)$. The deflection vector, $\boldsymbol{\delta}$, can be regarded as a change of location of an original point on the surface, (x, y, z), to its new position on the deformed surface, (x', y', z'), and is given by

$$\boldsymbol{\delta}(x, y) = \begin{Bmatrix} x' - x \\ y' - y \\ s'(x', y') - s(x, y) \end{Bmatrix} \tag{2.1}$$

The deflection vector is thus based upon a one-to-one mapping of all points in the closed set constituting the original surface to those on the deformed surface:

$$\begin{aligned} &\{(x, y, z) : x_1 \le x \le x_2; y_1 \le y \le y_2; z = s(x, y)\} \\ \rightarrow\ &\{(x', y', z') : x'_1 \le x' \le x'_2; y'_1 \le y' \le y'_2; z' = s(x', y')\} \end{aligned} \tag{2.2}$$

Such a map can be geometrically represented by the transformation

$$\begin{Bmatrix} x' \\ y' \\ s'(x', y') \end{Bmatrix} = \mathbf{T}(x', y', z' : x, y, z) \begin{Bmatrix} x \\ y \\ s(x, y) \end{Bmatrix} \tag{2.3}$$

Since the mean surface of most wing-like structures is essentially flat, the deflection at each point can be approximated by the displacement normal to the original surface,

$$\delta(x, y) = z' - s(x, y), \tag{2.4}$$

as shown in Fig. 2.1. In such a case, the deformed mean surface may not turn out to be flat, but can have a local curvature due to shear, twist, and spanwise and chordwise bending.

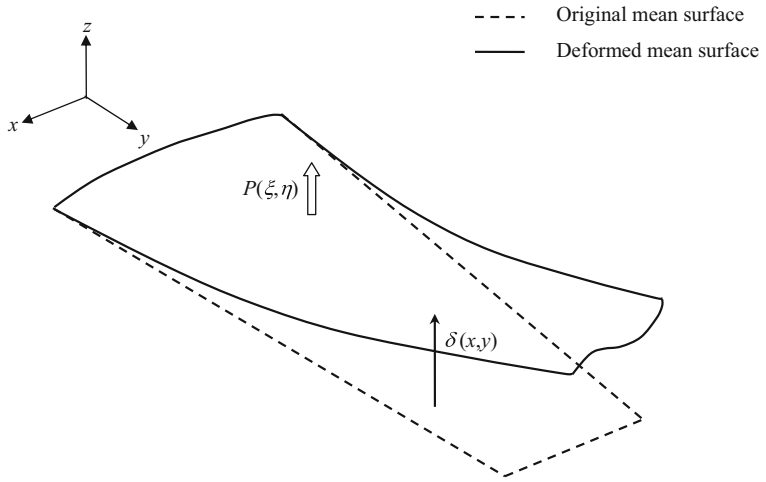

Fig. 2.1 Deformation of a wing-like structure under a concentrated load

The transformation matrix, $\mathbf{T}$, in Eq.(2.3) produced by a general loading must obey the material properties called *constitutive relationships*, and is also subject to the geometric constraints (also called kinematical relationships, compatibility requirements, or boundary conditions) on the structure. For a linearly elastic structure, the constitutive relationships take the form of a linear stress–strain behavior, such as

$$\boldsymbol{\tau} = \mathsf{C}\boldsymbol{\epsilon}, \tag{2.5}$$

where $\boldsymbol{\tau}$ and $\boldsymbol{\epsilon}$ are the stress and strain vectors, respectively, experienced by an infinitesimal structural element, and C denotes the matrix comprising the material properties. The linear stress–strain behavior of the material produces a linear relationship between the load and displacement of the structure, given by:

$$\boldsymbol{\delta}(x, y) = \mathbf{R}(x, y : \xi, \eta)\mathbf{P}(\xi, \eta), \tag{2.6}$$

where $\mathbf{R}(x, y : \xi, \eta)$ is the matrix of *flexibility influence-coefficient* functions (also called *Green's functions*). By applying linear superposition, Eq. (2.6) can be extended for the case of a continuously distributed load per unit area, $\mathbf{p}(\xi, \eta)$, as follows:

$$\boldsymbol{\delta}(x, y) = \iint_s \mathbf{R}(x, y : \xi, \eta)\mathbf{p}(\xi, \eta)\mathrm{d}\xi\,\mathrm{d}\eta. \tag{2.7}$$

Unfortunately, the flexibility influence-coefficient functions are rarely available in a closed form for any but the most simple structures. Therefore, numerical approximations must be made for the integral relationship given by Eq. (2.7). Such approximations are based upon a discretization of Eq. (2.7), whereby a continuous structure with infinitely many degrees of freedom is converted into an equivalent finite dimensional form. For example, the mean surface can be approximated by

n flat elemental panels of individual dimensions, $(\Delta\xi_i, \Delta\eta_i), i = 1 \ldots n$. The load distribution on the jth panel is then approximated by an average generalized load, $\mathbf{P}_j = \mathbf{p}(\xi, \eta)\Delta\xi_j \Delta\eta_j$ acting at a given *load point* (such as the panel centroid) in each panel. Similarly, the displacement, $\boldsymbol{\delta}(x, y)$, averaged over the ith panel is taken as the average deflection vector, $\boldsymbol{\delta}_i$, at a given *collocation point*, $(x_i, y_i), i = 1 \ldots n$. The discretized load–displacement relationship is then given for the ith panel as follows:

$$\boldsymbol{\delta}_i = \sum_{j=1}^{n} \mathbf{R}_{ij}\mathbf{P}_j \; ; i = 1 \ldots n \; . \tag{2.8}$$

Often, the individual elements of the displacement and load vectors are identified as *generalized displacements*,

$$\boldsymbol{\delta}_i = \begin{Bmatrix} q_{1i} \\ q_{2i} \\ q_{3i} \end{Bmatrix}, \tag{2.9}$$

and *generalized loads*,

$$\mathbf{P}_i = \begin{Bmatrix} Q_{1i} \\ Q_{2i} \\ Q_{3i} \end{Bmatrix}, \tag{2.10}$$

respectively, corresponding to the individual degrees of freedom at each point. Then Eq. (2.8) collected for all points takes the following vector-matrix form:

$$\mathbf{q} = \mathsf{R}\mathbf{Q} \, , \tag{2.11}$$

where the $3n \times 3n$ influence-coefficient matrix, R, consists of $\mathbf{R}_{ij}$ as its elements. Here, we note that $\mathbf{P}_i$ denotes the vector of all generalized loads (Q_{1i}, Q_{2i}, Q_{3i}) acting on the ith panel, while $\mathbf{Q}$ is the generalized loads vector for the entire structure derived by collecting all the generalized loads acting on all the panels. Similarly, the generalized displacement vector on the ith panel, $\boldsymbol{\delta}_i$, is to be distinguished from the overall generalized displacement vector of the structure, $\mathbf{q}$.

By making simplifying assumptions for a typical aircraft, the number of generalized coordinates can be significantly reduced. Such idealizations include chordwise rigidity, plate or beam-shaft approximations, and negligible streamwise loading on the structure. Due to their smaller dimensions and high stiffnesses, control surfaces are modeled simply by rotating angles about rigid hinge axes. Various definitions of the generalized loads and generalized displacements are possible, depending upon the idealizations and constitutive relationships used in deriving Eq. (2.11). There are also various alternative techniques for deriving the load–displacement relationship of Eq. (2.11) from constitutive relations and structural constraints. These include the *lumped parameters approximation*, the *finite-element method* (FEM) (or *Galerkin*

method), the *assumed modes* (or *Rayleigh–Ritz*) method, and the *boundary-element method*. Of these, the FEM is the most commonly employed due to its ease of implementation and modeling efficiency. We shall have the occasion to consider some examples of the FEM modeling a little later.

The influence-coefficient matrix,

$$\mathsf{R} = \begin{pmatrix} R_{11} & R_{12} & \cdots & R_{1N} \\ R_{21} & R_{22} & \cdots & R_{2N} \\ \vdots & \vdots & \vdots & \vdots \\ R_{N1} & R_{N2} & \cdots & R_{NN} \end{pmatrix}, \tag{2.12}$$

with $N = 3n$, consists of influence coefficients, R_{ij}, which are defined as the ith generalized *virtual coordinate*, δq_{ij}, produced by an isolated generalized load at a given point, Q_j,

$$\delta q_{ij} = R_{ij} P_j. \tag{2.13}$$

A virtual coordinate is an arbitrary, infinitesimal deflection in any of the three possible directions at a given point due to an isolated generalized load, and must be compatible with any kinematical constraints of the structure. The actual generalized coordinate, q_i, is a sum of all the virtual coordinates, δq_{ij}, caused by the generalized load, Q_j, and is given by the ith row of Eq. (2.11),

$$q_i = \sum_{j=1}^{N} \delta q_{ij} = \sum_{j=1}^{N} R_{ij} Q_j. \tag{2.14}$$

Therefore, the discrete influence coefficient, R_{ij}, can be understood as the ith virtual generalized coordinate due to the jth *unit* generalized load. The *reciprocal principle* of a linear structure requires that the ith virtual coordinate due to the jth unit load is the same as the jth virtual coordinate caused by the ith generalized load, i.e.,

$$R_{ij} = R_{ji}, \tag{2.15}$$

which implies that the matrix R is symmetric.

In order to determine the generalized loads from the generalized displacements they actually produce an inversion of Eq. (2.11) is required as follows:

$$\mathbf{P} = \mathsf{K}\mathbf{q}, \tag{2.16}$$

where $\mathsf{K} = \mathsf{R}^{-1}$ is the generalized *stiffness matrix* of the structure. Both R and K must be nonsingular and symmetric matrices. The element of $[K]$, k_{ij}—called the *stiffness coefficient*—is the ith generalized *virtual load* due to the jth *unit* generalized displacement. The work done by a generalized virtual load,

$$\delta Q_i = k_{ij} q_j, \tag{2.17}$$

in producing a generalized displacement, q_j, is given by

$$U_{ij} = \int \delta Q_i \mathrm{d}q_j = \int k_{ij} q_j \mathrm{d}q_j = \frac{1}{2} k_{ij} q_j^2 = \frac{1}{2} \delta Q_i q_j . \tag{2.18}$$

When summed over all points on the structure, the net work done by all the static forces is the total *strain energy* stored in the structure, given by

$$U = \sum_{i=1}^{N} \sum_{j=1}^{N} U_{ij} = \frac{1}{2} \mathbf{Q}^T \mathbf{q} = \frac{1}{2} \mathbf{q}^T \mathsf{K} \mathbf{q} . \tag{2.19}$$

The strain energy is the potential energy responsible for restoring the structure to its original shape once the loading is removed, and its quadratic form given by Eq. (2.19) is an important consequence of the linear elastic behavior. Since the external forces must be balanced by equal and opposite internal forces for a static equilibrium, one can regard U as the net work done by the internal, restoring (or conservative) forces.

2.3 Beam-Shaft Idealization

Consider a thin, high aspect-ratio wing with an essentially flat mean surface. Let (x, y, z) be Cartesian coordinates, such that x is in the chordwise direction measured from the elastic axis, y in the spanwise direction along the elastic axis on the mean plane, and z is normal to the mean plane. Saint-Venant's theory [68] postulates that a point exists at each cross-section of a slender beam about which a twisting load will produce a pure twist and a free warping, but no bending deformation. Such a point is called the *shear center*. Conversely, if a vertical load P is applied directly at the shear center, it will only cause pure bending deformation without any twisting or warping of the beam. The *elastic axis* is the line joining the shear centers at all spanwise locations. Assuming there is no bending in the chordwise (x) direction, and that plane cross-sections remain plane in the deformed configuration, the resulting structural displacement at any given point from the original (undeformed) shape can be represented by a combination of the normal deflection of the elastic axis at the given spanwise station, $w(y)$, the twist angle of the section about the elastic axis, $\theta(y)$, and the in-plane warp angle, $\phi(y)$, as depicted in Fig. 2.2. The net vertical deflection at location (x, y) is thus given by

$$\delta(x, y) = w(y) + x \tan\theta(y) , \tag{2.20}$$

whereas the in-plane deformation due to warping is merely $x \tan\phi(y)$. Since the angles θ, ϕ are small, one can apply the approximation $\tan\theta \simeq \theta$ and $\tan\phi \simeq \phi$, leading to the linear relationship

$$\delta(x, y) = w(y) + x\theta(y) . \tag{2.21}$$

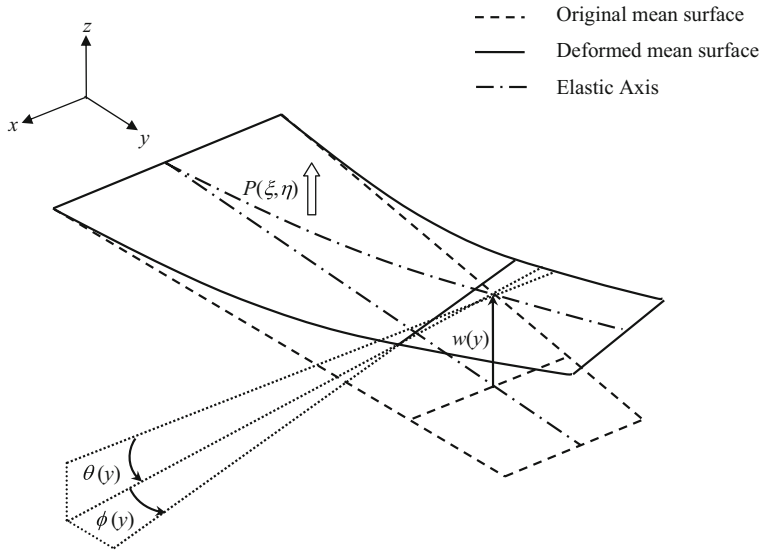

Fig. 2.2 Deformation of a thin wing of large aspect ratio under a concentrated normal load

The warp angle ϕ is inconsequential for aerodynamic loading, thus we have no need to model it any further. Since the structure is assumed to be linearly elastic, the load and displacement are linearly related by

$$\delta(x, y) = R(x, y : \xi, \eta)P(\xi, \eta), \tag{2.22}$$

where $R(x, y : \xi, \eta)$ is the flexibility influence-coefficient function (Green's function). By applying linear superposition, Eq. (2.22) can be extended for the case of a continuously distributed, normal load per unit area (pressure), $p(\xi, \eta)$, as follows:

$$\delta(x, y) = \iint_s R(x, y : \xi, \eta)p(\xi, \eta)\mathrm{d}\xi\mathrm{d}\eta. \tag{2.23}$$

The constitutive relations of the bending and twisting deformations are separately derived by considering a segment of the structure. For this purpose, the spanwise direction y is taken along the elastic axis, and bending deflection, $w(y)$ measured normal to the mean surface (called *neutral axis*) as shown in Fig. 2.3a. The kinematics (or compatibility) of the bending and shearing deformations is based upon the assumption that an originally plane section normal to the neutral axis must remain plane after deformation. However, this section can undergo a rotation due to shear deformation (shearing strain), $\beta(y)$, such that the section is no longer normal to the neutral axis. The bending slope, $w'(y)$, and the rotation angle due to shear, $\beta(y)$, thus collectively produce the net rotation, $\alpha(y)$, according to the following kinematical relationship:

$$\alpha = w' - \beta. \tag{2.24}$$

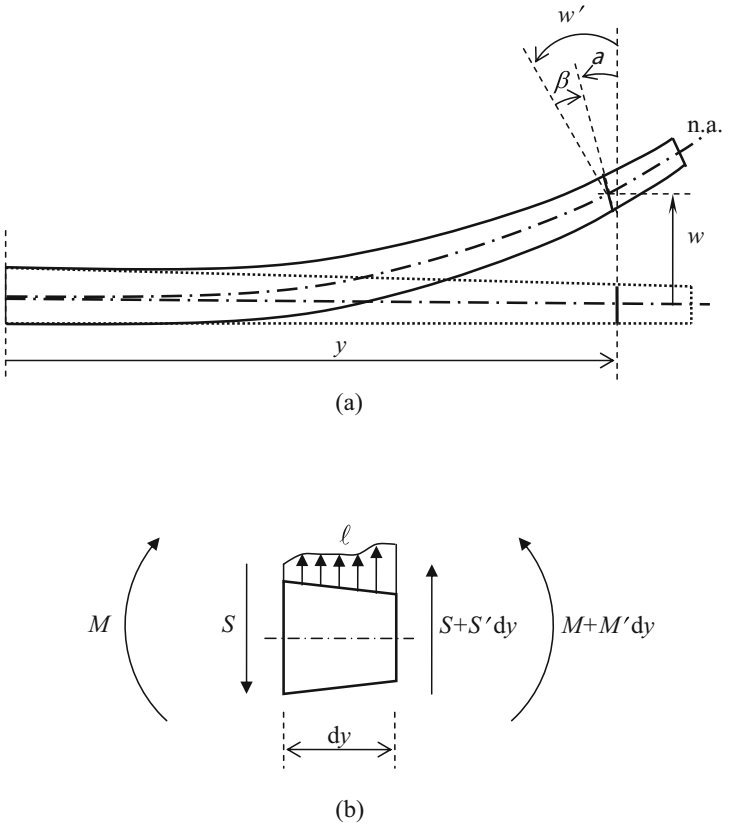

Fig. 2.3 Beam deflection geometry and static equilibrium of a beam segment

Equilibrium of a beam segment of infinitesimal length, $\mathrm{d}y$, with a static lift load per unit span, $\ell(y)$, requires an internal shear force, $S(y)$, and bending moment, $M(y)$, in order to balance the external load, $\ell(y)$, as shown in Fig. 2.3b. Neglecting second and higher order terms of $\mathrm{d}y$ results in the following linear equilibrium equations:

$$-S' = \ell, \tag{2.25}$$

$$S + M' = 0. \tag{2.26}$$

The bending and shear constitutive relationships of a material with Young's modulus of elasticity, E, and shear modulus, G, are the following:

$$\alpha' = \frac{M}{EI}, \tag{2.27}$$

$$\beta = \frac{S}{GK}, \tag{2.28}$$

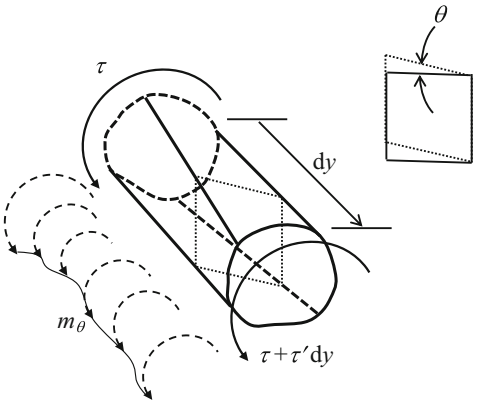

Fig. 2.4 Twisting of a slender shaft at a spanwise station, y

where $I(y)$ is the area moment of inertia and $K(y)$ the shearing constant of the beam cross-section. The quantity $EI(y)$ is called the bending stiffness and $GK(y)$ the shearing stiffness of the local beam cross-section. Substitution of Eqs. (2.27), (2.28), and (2.24) into Eqs. (2.25) and (2.26) results in the following differential equations for the beam:

$$\left(EI\alpha'\right)'' = \ell, \tag{2.29}$$

$$\left(EI\alpha'\right)' + GK\left(\alpha - w'\right) = 0, \tag{2.30}$$

which must be solved for $\alpha(y)$ and $w(y)$, subject to the boundary conditions of the structure. The net strain energy of the wing semispan idealized as a beam of length $b/2$ is then given by

$$U = \frac{1}{2}\int_0^{b/2} EI\left(\alpha'\right)^2 \mathrm{d}y + \frac{1}{2}\int_0^{b/2} GK\left(\alpha - w'\right)^2 \mathrm{d}y. \tag{2.31}$$

For thin, slender structures, the shear deformation, $\beta(y)$, can be neglected in comparison with the bending slope, $w'(y)$, leading to the following *Euler–Bernoulli* beam equation:

$$\left(EIw''\right)'' = \ell, \tag{2.32}$$

which must be solved for bending deflection, $w(y)$, subject to the boundary conditions. The net bending strain energy is now simply the following:

$$U = \frac{1}{2}\int_0^{b/2} EI\left(w''\right)^2 \mathrm{d}y. \tag{2.33}$$

Wherever possible to apply, Euler–Bernoulli assumptions are extremely valuable due to the simplicity of the resulting model.

For a slender, shaft-like structure (Fig. 2.4), the twisting deformation, $\theta(y)$, by shear of an originally straight edged element, is related to the local twisting moment, $\tau(y)$, about the elastic axis by Saint-Venant's theory [68] as follows:

$$\tau = GJ\theta', \tag{2.34}$$